REPORT DOCUMENTATION PAGE

AFRL-SR-AR-TR-07-0314

Public reporting burden for this collection of information is estimated to average 1 hour per response, including the time for reviewing instructions, data needed, and completing and reviewing this collection of information. Send comments regarding this burden estimate or any other aspect of t this burden to Department of Defense, Washington Headquarters Services, Directorate for Information Operations and Reports (0704-0188), 121 4302. Respondents should be aware that notwithstanding any other provision of law, no person shall be subject to any penalty for failing to comp valid OMB control number. **PLEASE DO NOT RETURN YOUR FORM TO THE ABOVE ADDRESS.**

1. REPORT DATE *(DD-MM-YYYY)*	2. REPORT TYPE	3. DATES COVERED *(From - To)*
15 July, 2007	Final Performance Report	January 15, 2004 –December 31, 2006

4. TITLE AND SUBTITLE: Piezoelectric Tailoring with Enhanced Electromechanical Coupling for Concurrent Vibration Control of Mistuned Periodic Structures

5a. CONTRACT NUMBER

5b. GRANT NUMBER
FA9550-04-1-0054

5c. PROGRAM ELEMENT NUMBER

6. AUTHOR(S)
Kon-Well Wang

5d. PROJECT NUMBER

5e. TASK NUMBER

5f. WORK UNIT NUMBER

7. PERFORMING ORGANIZATION NAME(S) AND ADDRESS(ES)

Dr. Kon-Well Wang
157E Hammond Building
The Pennsylvania State University
University Park, PA 16802

8. PERFORMING ORGANIZATION REPORT NUMBER

9. SPONSORING / MONITORING AGENCY NAME(S) AND ADDRESS(ES)
Air Force Office of Scientific Research
875 N Randolph Street
Arlington, VA 22203-1768
Dr Victor Giurgiutiu/NA

10. SPONSOR/MONITOR'S ACRONYM(S)

11. SPONSOR/MONITOR'S REPORT NUMBER(S)

12. DISTRIBUTION / AVAILABILITY STATEMENT
Approved for public release; distribution unlimited

13. SUPPLEMENTARY NOTES

14. ABSTRACT

The objective of this research is to advance the state of the art of vibration control of mistuned periodic structures utilizing the electromechanical coupling and damping characteristics of piezoelectric networking. In this investigation, an active coupling enhancement approach through negative capacitance has been developed to increase the piezoelectric electromechanical coupling. Experiments were carried out to validate the delocalization concept of the piezoelectric network. It was verified that the vibration localization level in a mistuned periodic structure can be reduced by using the piezoelectric networking and further improved by the negative capacitance. The piezoelectric networking concept was further extended and investigated as an effective means for vibration suppression of mistuned bladed disks. An optimal network was analytically derived and the performance and robustness of the optimal network was analyzed numerically through Monte Carlo simulation. The analysis showed that the optimal network can effectively suppress vibration of bladed disk systems under multiple spatial harmonic excitations, and is effective for mistuned systems. The optimal network is also robust against variations in circuitry parameters. Experiments were performed to demonstrate the multiple spatial harmonic vibration suppression effect of the piezoelectric network on a coupled blade and disk system. The test results verified the analytical predictions and showed that the proposed approach is effective in suppressing multiple engine order excitations.

15. SUBJECT TERMS
Piezoelectric networking, vibration delocalization, vibration suppression, bladed disks, periodic structures

16. SECURITY CLASSIFICATION OF:			17. LIMITATION OF ABSTRACT	18. NUMBER OF PAGES: 33 (including this page)	19a. NAME OF RESPONSIBLE PERSON
a. REPORT	b. ABSTRACT	c. THIS PAGE			19b. TELEPHONE NUMBER *(include area code)*
UNCLASSIFIED	UNCLASSIFIED	UNCLASSIFIED			

PIEZOELECTRIC TAILORING WITH ENHANCED ELECTROMECHANICAL COUPLING FOR CONCURRENT VIBRATION CONTROL OF MISTUNED PERIODIC STRUCTURES

GRANT FA9550-04-1-0054
Final Report (January 15, 2004 – December 31, 2006)

Principal Investigator

Kon-Well Wang
Diefenderfer Chaired Professor in Mechanical Engineering
157E Hammond Building
The Pennsylvania State University
University Park, PA 16803
(814) 865-2183, FAX: (814) 863-7222

Table of Contents

20070910339

Objectives

The objective of this research is to advance the state of the art of vibration control of mistuned periodic structures utilizing the electromechanical coupling, damping, and active control characteristics of piezoelectric networking. The new ideas are (a) to develop novel methods for increasing the network *electromechanical coupling* effect so that more mechanical energy can be redistributed electronically and enhance delocalization (reduce vibration localization); (b) to develop new methodology so that we can achieve effective vibration suppression of mistuned periodic structures under forced excitation in an optimal manner.

Summary of Efforts

(a) In this investigation, an active coupling enhancement approach through negative capacitance is developed to increase the piezoelectric electromechanical coupling. The effect of the negative capacitance on the delocalization performance of the network is systematically analyzed through numerical simulation.

(b) Experiments are carried out to validate the delocalization concept of the piezoelectric network through actual circuitry design. Through experiment, it is verified that the vibration localization level in a nearly (mistuned) periodic structure can be reduced by using the piezoelectric networking. The negative capacitance can increase the electromechanical coupling coefficient of the piezoelectric transducers, and thus improve the delocalization performance of the network.

(c) The piezoelectric networking concept is further extended and investigated as an effective means for vibration suppression of mistuned bladed disks. The study is performed in two parts. In the first part, the bladed disk is modeled as a relatively simple multiple-blade periodic system. An optimal network is analytically derived and the performance and robustness of this optimal network is analyzed numerically through Monte Carlo simulation. The analysis shows that the optimal network can effectively suppress vibration of bladed disk systems for multiple harmonic vibration suppression, and is effective for mistuned systems. The optimal network is also robust against variations in circuitry parameters. The analytical study is

further extended to a more complex scenario with the consideration of the coupled blade-disk dynamics. A new multi-circuit piezoelectric network design is developed for vibration suppression. The optimal tuning is derived analytically. The performance and the robustness issues of the network are again evaluated using Monte Carlo simulation. The effect of negative capacitance on the system performance and robustness is also investigated.

(d) Experiments are performed to demonstrate the multiple harmonic vibration suppression effect of the piezoelectric network on a coupled blade and disk system. A traveling wave excitation system is built to simulate the engine order excitation. The experiments show that the piezoelectric network is effective in suppressing multiple engine order excitations.

Descriptions of Accomplishments/New Findings

Part I: Vibration delocalization study

A basic piezoelectric network configuration utilized in this investigation is shown in Figure 1. In general, with piezoelectric patches mounted on or embedded in the substructures, an inductive circuit (*LC* shunt) can absorb significant amount of vibration energy from the substructure to which it is attached and store that portion of energy in the electrical form. While in most cases directly increasing the mechanical coupling between substructures is difficult to achieve due to various design limitations, one can easily introduce strong electrical coupling, such as connecting the *LC* shunts with interconnected capacitors, to create a new wave channel. With this coupled piezoelectric circuit design, the otherwise localized vibration energy in a mistuned periodic structure can now be transferred into electrical energy, and this energy can propagate in the integrated system through the newly created electro-mechanical wave channel with strong electrical coupling. This idea stems from previous findings on multi-coupled mistuned periodic structures, and will "destroy" the intrinsic mechanism for vibration localization.

The recent investigation has shown that while the piezoelectric networking idea is promising, the effectiveness of the treatment is limited by the level of electromechanical coupling of the piezoelectric patches. From observing Figure 1, one can see that since the electrical coupling established through the external capacitors (C_a) virtually has no limits, the bottleneck of the piezoelectric network is the electromechanical coupling, i.e. how much mechanical energy can be transferred into electrical energy. For most of the cases investigated in previous studies, the electromechanical coupling coefficient is not high enough to ensure that all the modes be significantly delocalized. In other words, while the degrees of localization of the modes were reduced with the treatment, the improvements in some modes were marginal. This coupling coefficient is in general difficult to change with only passive designs. An innovative method is needed to increase the coupling coefficient so that the mechanical energy can be better redistributed and delocalized.

It is well known that the electromechanical coupling coefficient is a function of various factors, such as the host structure stiffness, the piezoelectric material property, and the size and location of the piezoelectric patch. In theory, one can increase the coupling through reducing the host structure stiffness. However, it could be very difficult to tailor the mechanical structure stiffness in real applications. The effectiveness of varying the piezoelectric patch size and location is also limited. On the other hand, one can effectively enhance the electromechanical coupling coefficient by changing the piezoelectric patch capacitance [Tang and Wang, 2001]. In this research, we introduce the ***negative capacitance*** element concept to achieve such a purpose. Preliminary investigation by the investigator on general electromechanical coupling enhancement using negative capacitance has shown promising results [Tang and Wang, 2001]. By connecting a negative capacitance in series with the piezoelectric material, the overall apparent capacitance is increased, resulting in a much larger electromechanical coupling coefficient. Although the negative capacitance cannot be realized passively, one can easily use an operational amplifier to form a negative impedance converter circuit [Horowitz and Hill, 1989]. In this case, the power consumption is low and it is much easier to implement than mechanical tailoring.

In this task, network configurations with negative capacitance are created based on physical principles. The system mathematical model, consisting of a mistuned periodic structure and piezoelectric networks, is developed to synthesize the required negative capacitance. As an example to examine the feasibility of the idea, the system in Figure 1 is first used. The system equations of motion can be derived using Hamilton's principle,

$$m\ddot{q}_j + c\dot{q}_j + k(1+\Delta f_j)q_j + k_c(q_j - q_{j-1}) + k_c(q_j - q_{j+1}) + \kappa_1 Q_j = F_j \qquad (1)$$

$$L\ddot{Q}_j + k_p Q_j + k_a(Q_j - Q_{j-1}) + k_a(Q_j - Q_{j+1}) + \kappa_1 q_j = 0 \qquad (j = 1, 2, \cdots, N) \quad (2)$$

Here, m, c, and $k(1+\Delta f_j)$ are mass, damping, and stiffness of the j-th substructure. In this example, the mistuning is assumed to be on substructure stiffness. k is the nominal stiffness, Δf_j is a small random number (often referred to as the mistuning ratio) with zero mean, and k_c is the coupling stiffness between substructures. q_j is the mechanical displacement of the j-th substructure, F_j is the corresponding external disturbance, Q_j is the electrical charge flow through the network branch attached to the j-th substructure, and the cross coupling term κ_1 reflects the electromechanical energy conversion capability of the piezoelectric patch. It is this electromechanical coupling effect that causes the vibration energy to be transformed into electrical energy. L is the inductance value and k_p is the inverse of the capacitance value of the j-th piezoelectric patch. k_a is the inverse of the coupling capacitance, which is the electrical "spring" for electrical coupling among the subsystems. The combined effect of these electronic components will form an *electromechanical wave channel* between the additional electrical coordinates, which will be used to eliminate vibration localization.

From observing the system model, we can see that the generalized electromechanical coupling coefficient ($\xi = \kappa_1 / \sqrt{k k_p}$), can be increased by introducing a negative capacitance. When the negative capacitance is added in series to the piezoelectric element in the network, the inverse of the total capacitance in each branch of the piezoelectric networks becomes $\hat{k}_p = k_p - \tilde{k}_p$, where $\tilde{k}_p$ is the inverse of negative capacitance added. The generalized electromechanical coupling coefficient when the

negative capacitance is applied becomes $\xi = \kappa_1 / \sqrt{k\hat{k}_p}$. Since $\hat{k}_p$ is less than k_p, it is obvious that the generalized electromechanical coupling coefficient (ξ) can be increased by the treatment. To ensure system stability, a limit on the negative capacitance can be derived, which is governed by maintaining the positive definiteness of the system generalized stiffness matrix $\begin{bmatrix} k & \kappa_1 \\ \kappa_1 & \hat{k}_p \end{bmatrix} > 0$, meaning $k\hat{k}_p > \kappa_1^2$ or $\xi < 1$.

To validate the proposed concept, experimental effort is performed, with the overall setup shown in Figure 2. A mistuned bladed disk is vertically bolted at the hub disk center to a fixture on the isolation table. A shaker is used to excite the bladed disk through a stinger attached to the disk hub. Tip displacements of the blades are measured by a laser vibrometer (OFV-303, Polytec Germany). The laser vibrometer measures displacements by using the fringe counting technique, and converts the displacement information into a voltage related output (calibrated in μm/Volt or 10^{-6} meter/Volt). This voltage related output is captured by an HP35665A analyzer. The resolution of the vibrometer could be as high as 0.5 μm/Volt. The laser vibrometer is mounted on two perpendicular stages (X-Y stages as shown in Figure 2), which, controlled by LabVIEW programs, can precisely locate the measurement point on each blade tip.

The design of the bladed disk specimen was provided by the Wright Paterson Air Force Research Lab. It is a periodic structure with an overall diameter of 1 ft, consisting of a hub and 18 equally spaced cantilevered blades (length 4.25", width 0.305", thickness 0.125"), fabricated from standard aluminum alloy. The hub has a hole at the center, so that the blade disk could be securely bolted to the fixture on the isolation table, as shown in Figure 2. Due to the limited accuracy of the manufacturing process, the bladed disk is inherently mistuned. To build the piezoelectric network, each blade is attached with a piezoelectric patch (type 5A, APCI, Ltd.) at the root of the blade. The bonding process of the piezoelectric patches, and the possible slight difference among the patches themselves both contribute to the mistuning of the whole mechanical system (bladed disk with piezoelectric patches). Hereafter, the term *mistuned bladed disk*

actually refers to the original mistuned bladed disk with all the 18 piezoelectric patches attached to it. The patches have negative electrodes wrap-up design, which provides more effective bonding and more convenient wiring. The patches are isolated from the aluminum blades because the negative capacitance circuits must be located between the piezoelectric patches and the ground. The capacitance of the piezoelectric patches is measured to be $3.3nF$ (nano Farad).

Blade amplitudes for different cases are compared to evaluate the delocalization performance of the piezoelectric networks. Figure 3 plots the perturbation of blade amplitudes (subtracting the minimum amplitude among all substructures from each substructure's amplitude) when the mistuned bladed disk is under resonant excitation, with a circuit frequency tuning f_e = 212 Hz. When negative capacitance circuits are added into the piezoelectric network, the new resonant frequencies are re-identified, and the excitation frequency is adjusted accordingly. From reviewing these results, it is clear that the blade amplitude variation is significantly reduced with the piezoelectric network and the delocalization effect can be further improved by adding the negative capacitance circuits. Figure 4 shows the corresponding standard deviations of the amplitudes for different f_e values. It can be observed that, in general, under all 6 different circuit frequency tunings, localization is reduced for Case 3 (piezoelectric network with negative capacitance) when compared with Case 2 (piezoelectric network without negative capacitance). The decrease trend of the standard deviations from Case 1 (no treatment) to Case 3 indicates that vibration amplitudes become more and more evenly distributed. The fact that the conclusion is similar for all six f_e values indicates that the approach is robust against circuitry uncertainties. These results show that the delocalization ability of the piezoelectric network is significantly improved by the integrated negative capacitance circuits.

Part II: Vibration suppression study

Based on the previous promising results, the piezoelectric network concept is extended to forced vibration scenario. Here we focus on the vibration suppression in bladed

disks. As a class of cyclically periodic structures, modern bladed disk systems in turbo-machinery are especially sensitive to mistuning, and thus are very susceptible to localization. The effect of mode localization can result in large forced vibration amplitude when the rotating bladed disks are under harmonic aerodynamic loading (known as engine order excitation). The large forced response caused by mistuning can lead to accelerated fatigue and failure of engine components. Therefore, an effective means for vibration suppression is needed.

The analytical study provides a comprehensive understanding of the piezoelectric networking for effective multiple harmonic vibration suppression of mistuned bladed disks. The analysis consists of two parts. In the first part, the bladed disk is modeled as a multi-blade periodic system with disk dynamics neglected. The model in Figure 4(a) is used. In this model, each blade is modeled as a cantilever beam. Coupling through the disk is modeled by the spring connecting adjacent blades. The piezoelectric network is shown in Figure 4(b). Identical piezoelectric patches are attached to each blade. The piezoelectric network is constructed as follows: first an inductor (L) and a resistor (R) are connected to each piezoelectric patch (with electric capacitance C) in order to form a resonant LRC circuit. For reasons to be clear later, these shunts are then networked through passive capacitors (C_a).

The equation of motion for the j^{th} blade without the piezoelectric circuits is,

$$m\ddot{q}_j + c\dot{q}_j + (k + \Delta k_j)q_j + k_c(2q_j - q_{j-1} - q_{j+1}) = f_j \tag{3}$$

And the equations of motion for the j^{th} blade integrated with the j^{th} circuit branch are,

$$m\ddot{q}_j + c\dot{q}_j + (k + \Delta k_j)q_j + k_c(2q_j - q_{j-1} - q_{j+1}) + k_1 Q_j = f_j \tag{4}$$

$$L\ddot{Q}_j + R\dot{Q}_j + k_2 Q_j + k_a(2Q_j - Q_{j-1} - Q_{j+1}) + k_1 q_j = 0 \tag{5}$$

To design the absorber circuitry, let us start with the tuned case, that it, let Δk_j =0, and neglect structural damping c since bladed disk systems usually have very light damping. One can apply U-transformation [Tang and Wang, 1999] to de-couple the above equations:

$$m\ddot{x}_j + [k + 2k_c(1-\cos((j-1)\theta))]x_j + k_1 y_j = h_j \tag{6}$$

$$L\ddot{y}_j + R\dot{y}_j + [k_2 + 2k_a(1-\cos((j-1)\theta))]y_j + k_1 x_j = 0 \tag{7}$$

Here, j stands for the j^{th} spatial harmonic. Following the procedure in [Tang and Wang, 1999], one can derive the analytical solution for the optimal circuitry parameter tuning. For comparison purpose, we also examine the traditional absorber design, which is composed of individual LCR shunt circuits without coupling capacitance C_a, the optimal inductance tuning is:

$$L_{trad\_opt} = \frac{mk_2}{k + 2k_c(1-\cos((j-1)\theta))} \tag{8}$$

In this case, it is obvious that the optimal tuning is dependent on the spatial harmonic number j. In other words, the non-networked traditional absorber can only be optimally designed to suppress a specific spatial harmonic excitation. By applying the coupling capacitance and forming the network, one can derive the optimal inductance:

$$L = \frac{m[k_2 + 2k_a(1-\cos((j-1)\theta))]}{k + 2k_c(1-\cos((j-1)\theta))} \tag{9}$$

The expression in Eq. (9) is still j-dependent. However, by properly tuning the coupling capacitance C_a (note that k_a=1/C_a), such that $k_a = \frac{k_2 k_c}{k}$, the optimal L will become,

$$L_{ntwk\_opt} = \frac{mk_2}{k} \tag{10}$$

It is thus obvious that this expression is no longer j-dependent, meaning that it will be effective for all spatial harmonic excitations. For resistance tuning, previous study [Zhang and Wang, 2002] has found that the system performance is not very sensitive to small perturbation in the resistance, thus a single resistance value is used for all spatial harmonics by taking j=1. Thus, $R^* = \frac{k_1}{k}\sqrt{2mk_2}$ for both the traditional absorber and optimal network design.

In Figure 6, we compare the multiple-harmonic vibration suppression effects of the traditional absorber and the optimal network for bladed disk under summation of engine

order excitations. For the traditional absorber, harmonic number j is arbitrarily picked to be j=2 in Eq. (8). In Figure 6, the maximum blade response of the baseline system without control is plotted in grey solid line, that with traditional absorber in black dotted line, and that with optimal piezoelectric network in black solid line. As one can see that the traditional absorber can only effectively suppress a few frequency-response peaks, and loses its effectiveness on others. Nevertheless, the optimal network can effectively suppress the vibration at all peaks. This is because the traditional absorber can only be optimally tuned to a specific harmonic, while the optimal network, through networking, can be tuned to suppress all spatial harmonics (i.e., harmonic independent).

The vibration suppression performance and robustness of the network are also investigated using Monte Carlo simulation for the mistuned bladed disk systems. A maximum blade response ratio between the 'with network' and 'without network' cases is defined, and the 95th percentile value from all the ratios is used as the *performance index* in evaluating the network performance.

The performance of the optimal network (without negative capacitance, ξ = 0.1) for mistuned bladed disk systems with random mistuning is shown as the solid line in Figure 7. Observing the solid line, when σ =0, i.e., when the bladed disk system is tuned, the performance index is 0.025, which means that with the network, the maximum blade response is reduced by 97.5%. As the mistuning level increases, the performance degrades, as seen in the increasing trend of the performance index. However, even with σ =0.08, which is considered as a quite large mistuning level, the performance index is still smaller than 0.12. This means the maximum blade amplitude is still reduced by approximately 88%. Such a result shows that our piezoelectric system, although designed based on tuned system, performs very well for mistuned system. The same approach is carried out to analyze the system with random mistuning in electrical elements and similar results can be concluded. That is, the system's performance is quite robust against moderate differences among the electrical circuitry parameters as well as that among the mechanical structural parameters.

The robustness of the network in terms of circuitry detuning is also investigated. Detuning means that the nominal values of a circuitry parameter in all local circuits are uniformly off-tuned by the same amount. Such detuning could be results of modeling or design errors, where the relative errors could be larger than those caused by random mistuning. Our study shows that the network's performance is not much affected by small to moderate detuning in circuitry parameters. An example is shown in Figure 8. Figure 8 shows small (-5%) to moderate (-10%) detuning effect in inductance. With -5% detuning and -10% detuning in the optimal circuitry, the circuit becomes non-optimal and the maximum blade response is increased by 7dB and 11dB. However, the overall amplitude reduction is still significant (over 40dB reduction) compared to the maximum response of the original mechanical system without network.

The effect of negative capacitance is also investigated. Here we consider three cases: without negative capacitance case where ξ=0.1 and with negative capacitance cases, where ξ=0.2 and ξ=0.3. It can be seen from Figure 7 that with negative capacitance (thus higher ξ), the performance index is lowered throughout the entire range of stiffness mistuning level. For example, with ξ =0.2, for mistuning level as large as σ =0.08, the performance index is below 0.02, meaning 98% reduction in the maximum forced response. Higher (ξ = 0.3) yields even better vibration suppression results. When circuitry parameter detuning is considered, results with negative capacitance are shown in Figure 9 with detuning in optimal circuitry frequency which is related to inductance. In these figures, with negative capacitance (thus higher electro-mechanical coupling), the performance index can be further reduced, not only making the network more robust against detuning around optimal tuning, but also making the network capable of tolerating a wider range of detuning. For example, if the performance satisfaction threshold is set at performance index equal to 0.05 in Figure 9, then without negative capacitance the detuning tolerance range in is roughly [0.8, 1.3]. On the other hand, with negative capacitance, for ξ =0.2, the circuitry frequency can be detuned within the range of [0.6, 1.5], and for ξ =0.3, the entire range [0.5, 1.5] can be used. Similar results can be obtained from the detuning study in other parameters.

The analysis is further extended to a more complex situation. In this case, we consider the coupled blade-disk dynamics. A new model is developed, as shown in Figure 10. This model, with the inclusion of the disk dynamics, can capture frequency veering characteristics of bladed disks, and is a better representation of the actual systems. In this new bladed disk model, assuming that the system has N blades, the system is first virtually partitioned into N repetitive identical bays, with each bay consisting of a sector of the disk (therefore, the whole disk is partitioned into N identical disk sectors), and a blade (as shown in Figure 10, the j^{th} bay is enclosed in the dotted frame). At each bay, the blade is modeled as a cantilever beam (marked with 'b', and referred to as the 'blade-model beam' hereafter), and for simplicity, the disk sector is also modeled as a cantilever beam (marked with 'd', and referred to as the 'disk-model beam' hereafter). The coupling mechanism of the system is modeled by two parts: spring k_s that emulates the coupling between the blade and disk (blade-disk coupling), and spring k_c that emulates the coupling between adjacent disk sectors (disk-disk coupling). Therefore, the inter-blade coupling is now implicitly modeled through the combination of the blade-disk coupling and disk-disk coupling. The model is cyclically symmetric with a ring type rigid base to provide clamping condition for those cantilever beams. It should be noted that Figure 10 only shows a portion of the system for illustration purpose. Assuming there are N bays, the 1^{st} bay is connected with the last bay (the N^{th}) to form a closed loop. The equations of motion are shown in Eq. (11) and Eq. (12).

$$m_b\ddot{x}_{bj} + k_b x_{bj} + c_1\dot{x}_{bj} + k_s(x_{bj} - x_{dj}) = f_{bj} \tag{11}$$

$$m_d\ddot{x}_{dj} + k_d x_{dj} + c_2\dot{x}_{dj} + k_s(x_{dj} - x_{bj}) + k_c(2x_{dj} - x_{dj+1} - x_{dj-1}) = f_{dj} \tag{12}$$

Here, m_b, k_b, c_1 (or m_d, k_d, c_2) are the mass, stiffness, and damping of the blade-model beams (or disk-model beams); k_s (or k_c) is the 'blade-disk' (or 'disk-disk') coupling spring stiffness; x_{bj} (or x_{dj}) is the generalized displacement of the j^{th} blade-model beam (or disk-model beam); f_{bj} (or f_{dj}) is the force on the j^{th} blade-model beam (or disk-model beam). The force used in the study is the engine order excitation. Engine order excitation applies the same forcing magnitude to each bay with a fixed phase difference between adjacent bays. For example, the force on the j^{th} blade-model beam can be

expressed in the form of: $f_{bj} = f_{b0} e^{i\theta(j-1)(E-1)}$, where f_{b0} is the forcing amplitude, $i = \sqrt{-1}$, $\theta = 2\pi / N$, N is the total blade number, E is the engine order number. The phase difference between adjacent bays is $\theta(E-1)$, which is determined by the engine order number E. In this study, the same engine order excitation formula is applied to the disk-model beams.

Figure 11 depicts an example frequency veering plot based on the new bladed disk model (tuned system). Frequency veering (more generally known as curve veering) refers to a phenomenon where two natural frequency loci converge and then veer apart without crossing each other at certain point as some parameter varies. In this example, frequency veering occurs as the natural frequencies are plotted versus the nodal diameter number of the tuned modes, and occurs at a region around nodal diameter number 4 and 5. It has been shown that frequency veering is related to the coupling between mode shapes, which could lead to localization when the structure is disordered [Pierre, 1988]. In bladed disk systems, frequency veering is associated with the interaction between the blade dominant modes and the disk dominant modes. Studies [Bladh et al., 2002; Kenyon et al., 2004] on the forced vibration of bladed disks have shown that frequency veering increases the sensitivity of the tuned system to mistuning. Consequently, frequency veering can lead to a much higher amplitude magnification factor compared to the situations where frequency veering does not occur (e.g., in the case where only the blade degrees-of-freedom are considered).

Figure 12 depicts the ratio between the modal amplitudes of the blade-model beams and the disk-model beams at each mode corresponding to Figure 11. Figure 12 shows that before veering, modes in the upper curve (squares) are blade dominant, while in the lower curve (diamonds) are disk dominant. After veering, the modes in the upper curve (diamonds) become disk dominant, while in the lower curve (squares), modes become blade dominant. Although for the modes in the veering region (with nodal diameter 4 and 5), the modal amplitude difference between the blade and disk are not as large as those in the off-veering region, still, one component (either blade or disk) is dominant.

From Figures 11 and 12, it is also observed that the blade dominant modes are clustered in natural frequencies around frequency 1.1, while disk dominant modes have a wider frequency span (from about 0.5 to 1.6). This characteristic captures one of the modal features of the bladed disk systems, where the blade dominant modes tend to be less affected by the nodal diameter (thus frequency curve is flatter versus nodal diameter), whereas the disk dominant modes tend to be more affected by the nodal diameter (thus frequency curve is steeper versus nodal diameter).

In this research, a new multi-circuit network architecture is developed to achieve effective vibration suppression for this bladed disk system. The bladed disk model with integrated new piezoelectric circuitry configuration is shown in Figure 13. This new network is constructed in the following fashion. First, piezoelectric patches are embedded to the root of each cantilever beam, as shown in Figure 13. The corresponding treatment on the corresponding actual bladed-disk system would be: on each blade, a piezoelectric patch is applied to the position close to the root of the blade (note that the blade is fixed to the disk); and on the disk, each piezoelectric patch is applied to each disk sector, at the root position of the sector (note that the disk is fixed to the rotating shaft, and is first virtually partitioned into N identical sectors as discussed in the previous section). On each blade-model beam, local damped absorber shunt circuit is formed by connecting the piezoelectric patch with an inductor (L_1) and a resistor (R_1). On each disk-model beam, a coupled circuit network is configured as shown in Figure 13 using L_2, R_2, C_2, and C_a. Here L_2, R_2 and the piezoelectric patch form a local shunt. Capacitor C_a is used to couple these local shunt circuits. The additional capacitor C_2 is added to cancel out some effects caused by the mechanical coupling k_s between the blade-model beam and the disk-model beam. The importance of these two capacitive elements will be clearer in the derivation of the optimal network for suppressing multiple harmonics. The equations of motion for the electro-mechanically integrated system in Figure 13 can be derived as:

$$m_b\ddot{x}_{bj} + k_b x_{bj} + c_1\dot{x}_{bj} + k_s(x_{bj} - x_{dj}) + k_{bp1}Q_{1j} = f_{bj} \tag{13}$$

$$L_1\ddot{Q}_{1j} + k_{pzt1}Q_{1j} + R_1\dot{Q}_{1j} + k_{bp1}x_{bj} = 0 \tag{14}$$

$$m_d\ddot{x}_{dj} + k_d x_{dj} + c_2\dot{x}_{dj} + k_c(2x_{dj} - x_{dj-1} - x_{dj+1}) + k_s(x_{dj} - x_{bj}) + k_{bp2}Q_{2j} = f_{dj} \tag{15}$$

$$L_2\ddot{Q}_{2j} + k_{pzt2}Q_{2j} + R_2\dot{Q}_{2j} + k_2Q_{2j} + k_a(2Q_{2j} - Q_{2j-1} - Q_{2j+1}) + k_{bp2}x_{dj} = 0 \tag{16}$$

Here, Eq. (14) is derived from the circuit branch on the j^{th} blade-model beam, and Eq. (16) is derived from the circuit branch on the j^{th} disk-model beam. In Eqs. (13) and (14), k_{bp1} (or k_{bp2}) are parameters related to the electro-mechanical coupling factors of the piezoelectric patches on the blade-model beams (or disk-model beams); L_1, R_1 (or L_2, R_2) are inductance and resistance in the circuit connected to piezoelectric patch on the blade-model beams (or disk-model beams). $k_{pzt1}=1/C_{pzt1}$ (or $k_{pzt2}=1/C_{pzt2}$) is the inverse of piezoelectric capacitance on the blade-model beams (or disk-model beams). $k_2=1/C_2$, is the inverse of the additional capacitance C_2; and $k_a=1/C_a$, is the inverse of coupling capacitance C_a; Q_{1j} (or Q_{2j}) is the charge flow across the piezoelectric patch on the j^{th} blade-model beam (or disk-model beam).

Due to the complexity of the system, it is very difficult to analytically derive the closed form optimal circuit parameter tuning from the original equations of motion in Eqs. (13)-(16). However, based on the observation from the analyses in Figures 11-12, it is reasonable to separate the design problem into two parts: (a) the blade-dominant case and (b) the disk-dominant case. In part (a), where the system dynamics are blade dominant, Eq. (13) can be approximated by neglecting the disk degree of freedom x_{dj}. In part (b), where the dynamics are disk dominant, Eq. (14) can be approximated by neglecting blade degree of freedom x_{bj}. Then by applying U-transformation, one can derive the optimal tuning analytically. The optimal tunings for circuits with L_1, R_1 are:

$$L_{1opt} = k_{pzt1}m_b/(k_b + k_s) \tag{17}$$

$$R_{1opt} = k_{bp1}\sqrt{2m_b k_{pzt1}}/(k_b + k_s) \tag{18}$$

For the circuit with L_2, R_2, C_2, and C_a, the inductance tuning is:

$$L_2 = \frac{[k_{pzt2} + k_2 + 2k_a(1-\cos((j-1)\theta))]m_d}{k_d + k_s + 2k_c(1-\cos((j-1)\theta))} \tag{19}$$

where j is the spatial harmonic. Equation (19) shows that this inductance tuning is dependent on the spatial harmonic j. However, if one tune the additional capacitor (C_2) and coupling capacitor (C_a) such that $k_2/k_{pzt2} = k_s/k_d$ and $k_a/k_{pzt2} = k_c/k_d$ are satisfied, one can obtain a solution that is independent of spatial harmonic j, as shown

in Eq. (20). Here, one can see that in order to obtain this solution, k_a and k_2 play very important roles.

$$L_{2opt} = k_{pzt2} m_d / k_d \tag{20}$$

The resistance tuning in the circuits on the disk-model beams is tuned to spatial harmonic j=1, as shown below:

$$R_{2opt} = k_{bp2} \sqrt{2 m_d k_{pzt2}} / k_d \sqrt{1 + k_s / k_d} \tag{21}$$

Figure 14 shows the comparison of the vibration suppression performances between the newly developed network (black solid line) and the 'traditional' absorber (grey solid line). The black dotted line is the forced response of the baseline bladed disk system without any treatment. The 'traditional' absorber design is referred to as simple uncoupled individual *LCR* circuits applied to each cantilever beam (regardless of representing blade or disk sector) in Figure 13, without C_2 and C_a elements. More specifically, for the blade-model beams, the circuits remain the same; for the disk-model beams, circuits with the same architecture as those used on the blade-model beams are applied here. The optimal inductance tuning for traditional absorber is dependent on spatial harmonic j, the mathematical expression of which is $L_{opt\_trad} = \dfrac{k_{pzt2} m_d}{k_d + k_s + 2k_c(1-\cos((j-1)\theta))}$. This means the traditional absorber can only be tuned to suppress a specific spatial harmonic (j) in engine order excitations. In Figure 14, the spatial harmonic j for the traditional absorber is arbitrarily chosen to be j=1. The force is a summation of all engine order excitations, thus contains multiple harmonics. It can be seen that compared to the traditional absorber, the optimal network is much more effective in suppressing multiple harmonics simultaneously, and as a result, the maximum responses are much lower.

The network performance for vibration suppression of mistuned bladed disks and the robustness issues are again evaluated using Monte Carlo simulation. The performance index is defined in the same way as the one previously used. Figure 15 shows the performance index versus mechanical mistuning. It can be seen that even at the largest mistuning level (σ = 0.08) the index is still below 0.11, which means over 89%

vibration reduction can be achieved over the entire mistuning range. Therefore, the network performs very well for vibration suppression of mistuned system as well.

The mistuning effect of the circuit parameters is also investigated. It is shown that the system performance is not affected too much by the mistuning. Within the 0-0.08 mistuning level considered, in all parameter cases, the study shows that about 75% or more reduction in the maximum blade response can be achieved. An example with mistuning in δ_{e1} (which is related to the inductance L_1) is shown in Figure 16.

The detuning effect in the circuit parameters is also studied. It is shown that the network performance is not sensitive to most of the parameters. The network shows more sensitivity in δ_{e2}, which is related to the inductance L_2. However, in such a situation, our study shows that negative capacitance can improve the system performance and robustness. Figure 17 shows an example. Figure 17 depicts the effect of negative capacitance with detuning in δ_{e2}. Here, negative capacitance is added to the circuits on the disk-model beams, therefore, ξ_1 remains at the nominal value (0.1), and ξ_2 is increased from the default value 0.1 to 0.2. It is shown in the figure that the performance index is generally reduced throughout the detuning range. Significant reduction in the index is achieved at the larger detuning levels. For example, for -20% detuning, the original index is about 0.7 without negative capacitance, and is reduced to only 0.35 with negative capacitance. With negative capacitance, the slopes of the curve become smaller for either positive detuning or negative detuning. Also, larger detuning range can be tolerated if one has a pre-set performance index threshold. For example, if the performance threshold is set at index 0.25, the tolerable detuning range for the case without negative capacitance is about [-5%, +8%], while with negative capacitance, for ξ_2=0.2, the tolerance range can be increased to about [-15%, +20%].

The vibration suppression effect of the piezoelectric network is then examined through experiment. The baseline bladed disk model system with piezoelectric patches is shown in Figure 18. This system is designed according to the new bladed disk model

presented in Figure 10. In this periodic system, there are twelve aluminum beams forming six bays, with each bay consisting of a shorter beam, which simulates the blade dynamics, a longer beam which simulates the disk dynamics, and two connecting springs with the longer one corresponding to k_c in Figure 10 and the shorter one corresponding to k_s. Identical piezoelectric transducers (patch type) are bonded to the root of each beam on both sides, with one functioning as an exciter to provide engine order excitation for the structure (transforming electric energy to mechanical energy); and the other functioning as a part of the piezoelectric circuitry network (transforming mechanical vibration energy into electrical form). This periodic bladed disk system is intrinsically mistuned due to many sources that can cause differences among bays, including the variations in the lengths of beams, the clamping conditions, the piezoelectric patches' bonding conditions, the spring fixing conditions, etc.

The overall experiment setup is shown in Figure 19. This testing system includes the bladed disk structure, a traveling wave excitation system, a measurement system, and a piezoelectric circuitry. The traveling wave excitation system is designed to simulate the engine order excitation force. The excitation force on the j^{th} blade-model beam (or disk-model beam) can be expressed as: $F_j = F_0 \cos(\omega t + (j-1)\phi)$, where $\phi = 2\pi E / N$, N=6, and E is the engine order number, E=0, ..., N/2. Displacement measurements are taken using six fiber optic sensors (Philtec D20) positioned in the close proximity of the tips of blade-model beams (shorter beams). The displacement data is acquired by the Simulink model and dSpace, and processed by a Matlab code.

Figures 20 to 23 compare the vibration suppression results of the network and of the traditional absorber. In each figure, the maximum blade response curve corresponding to the 'without circuit' case (i.e., the baseline mechanical system case) is the black dotted line, the grey solid line represents the 'with traditional absorber' case, and the 'with network' case is denoted by the black solid line. The maximum blade responses are obtained from all blades. Each figure uses one specific engine order excitation, E=0, 1, 2, 3. The maximum response ratios are also shown in these figures. This ratio

is defined by taking the division between the maximum response of with circuit case (with network or with traditional absorber) and that of the baseline mechanical system case. Therefore, the ratio indicates the vibration suppression effectiveness, with smaller value meaning more vibration reduction. For example, the ratio of 0.445 for engine order 0 ('with network') means that the maximum blade response is suppressed by 55.5% with the use of the network. Observing Figures 20 to 23, one can see that at engine order 0, the performance of the network and the traditional absorber is similar in terms of maximum response ratio. However, the ratios for traditional absorber are much higher than that for the network when the structure is under other engine orders (E=1,2,3). This is expected since the traditional absorber is tuned to engine order 0. The experimental results indicate that the piezoelectric network is effective for vibration suppression at all engine order excitations, and outperforms the traditional absorber that is only effective at one specific engine order excitation.

Personnel Supported

Other than the PI, Dr. K. W. Wang, the project has involved one Ph.D. students (H. Yu – graduating August 2007) and one Post-Doc Fellow (Dr. J. Zhang).

Publications

Yu, H., Wang, K.W., and Zhang, J., 2006, "Piezoelectric networking with enhanced electromechanical coupling for vibration delocalization of mistuned periodic structures – theory and experiment," *Journal of Sound and Vibration,* 295(1-2), pp. 246-265.

Yu, H., Wang, K.W., 2006, "Piezoelectric networks for vibration suppression of mistuned bladed disks," *Journal of Vibration and Acoustics*, accepted for publication.

Yu, H., Wang, K.W., 2006, "Piezoelectric networks for vibration suppression of mistuned bladed disks," *Proceedings of ASME International Mechanical Engineering Congress and Exposition (IMECE), IMECE2006-15067, November 5-10, Chicago, IL, USA.*

Yu, H., Zhang, J., Wang, K.W., 2004, "Experimental investigation of vibration delocalization of mistuned bladed disks utilizing piezoelectric circuitry design," *Proceedings of SPIE,* v 5386, *Smart Structures and Materials 2004-Damping and Isolation,* pp. 269-281.

Yu, H., Wang, K.W., 2004, "Piezoelectric networking with enhanced electromechanical coupling for vibration delocalization of mistuned periodic structures –theory and

experiment," *Proceedings of International Conference on Adaptive Structure Technology,* Bar Harbor, Maine, USA.
Yu, H, Wang, K.W., 2007, "Vibration suppression of mistuned coupled-blade-disk systems using piezoelectric circuitry network," submitted to ASME 2007 IDETC Conference, September 4-7, Las Vegas, Nevada, USA.

Yu, H., Wang, K.W., 2007, "Piezoelectric networks for vibration suppression of bladed disks," will be presented and published at The 18th International Conference of Adaptive Structures and Technologies, October 3-5, Ottawa, Canada.

Yu, H., 2007, *Piezoelectric Networking for Mode Delocalization and Vibration Suppression of Nearly Periodic Structures*, Ph.D. thesis, Penn State University.

Interactions/Transitions

This research is very relevant to AFOSR's mission, since the results can be applied to vibration control of various Air Force systems, such as space structures, satellite antennae, and bladed-disk assemblies (e.g., fans and compressors) in gas turbine engines. The PI, Dr. Wang, has had various interactions and technical discussions with Dr. Charles Cross and other researchers at the Wright-Patterson Air Force Research Lab (AFRL) on issues regarding fan structure implements and experimental set ups. Based on Dr. Cross' advice, the test specimen designed by the Wright-Patterson AFRL researchers was used in the Penn State delocalization test. Dr. Wang has also had communications with researchers at the Kirtland AFRL.

Honors/Awards

Dr. K. W. Wang is a Fellow of the ASME and the holder of the Diefenderfer Chair in Mechanical Engineering at Penn State. He is the recipient of the 2004 Penn State Engineering Society Premier Research Award. He will be receiving the ASME N. O. Myklestad Award for major innovative contribution to vibration engineering in 2007.

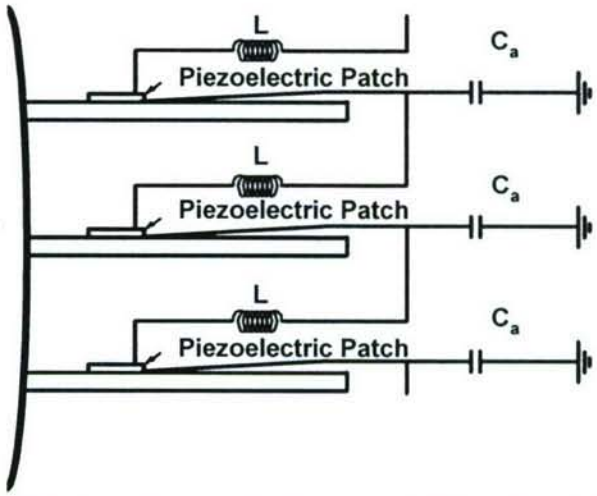

Figure 1. Periodic structure augmented with coupled piezoelectric circuits

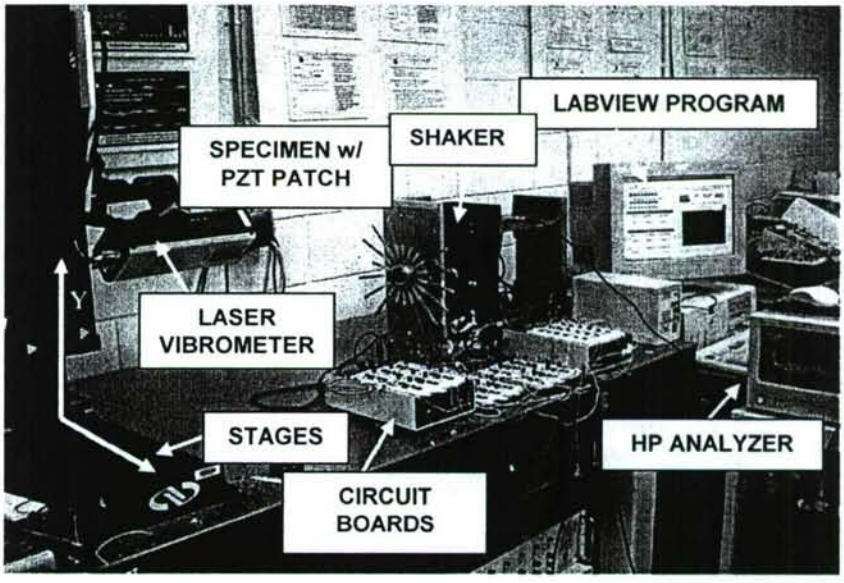

Figure 2. Overall test setup for vibration delocalization.

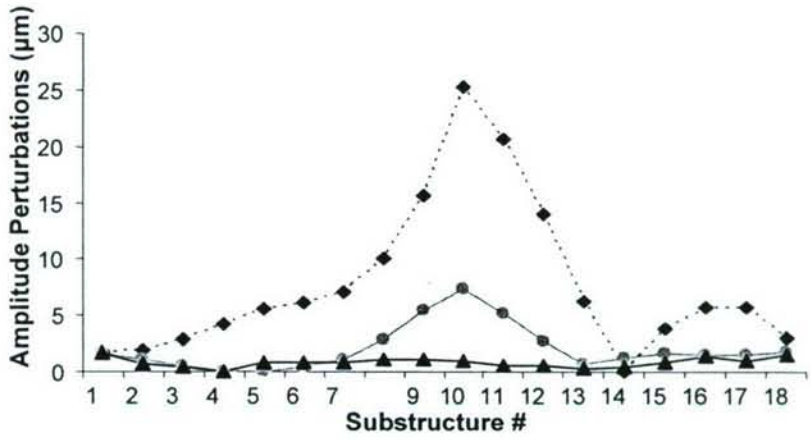

Figure 3. Experimental results: ♦: system without treatment; ●: system with piezoelectric network but without negative capacitance; ▲: system with piezoelectric network and with negative capacitance.

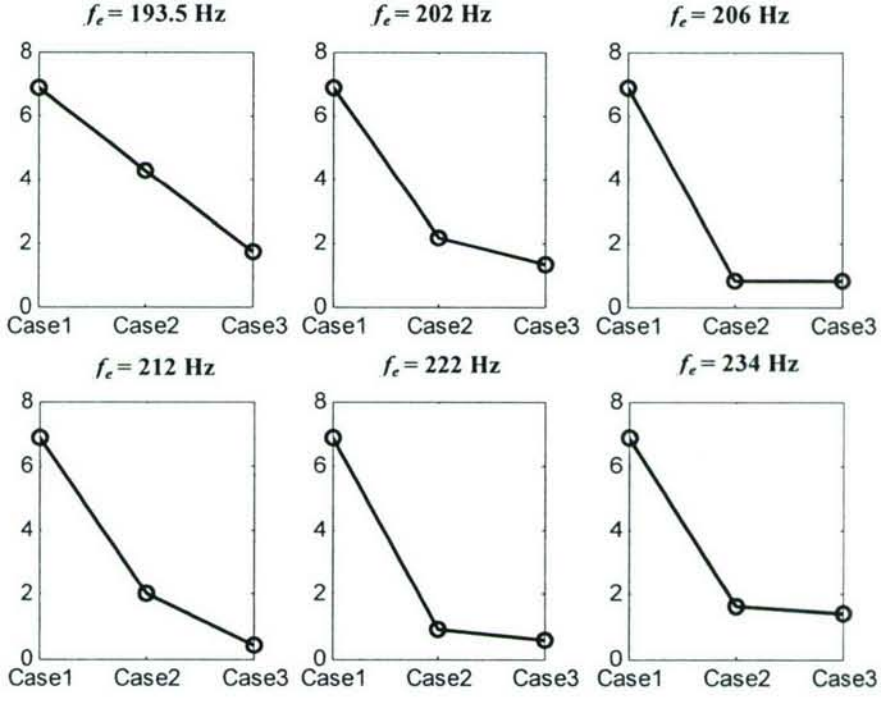

Figure 4. Standard deviations of blade relative amplitudes for Case 1 (mistuned bladed disk without network), Case 2 (with network) and Case 3 (with network augmented by negative capacitance). Vertical axis: standard deviation (unit: μm).

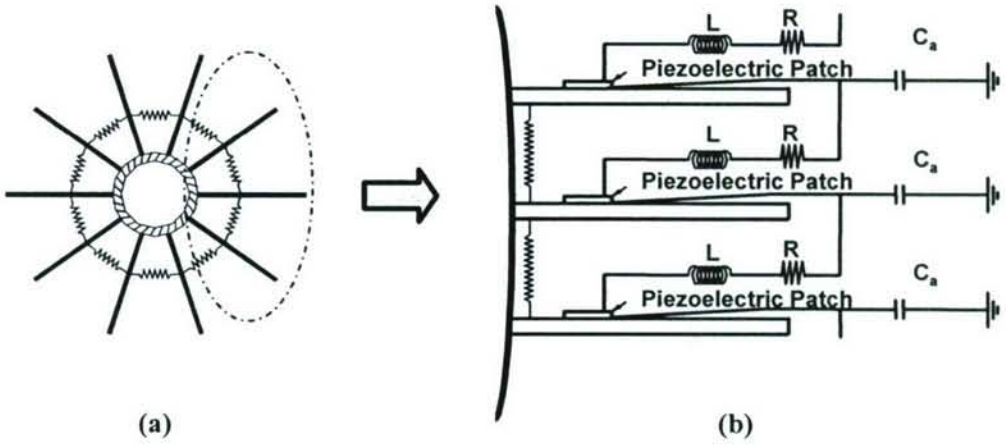

Figure 5. System schematics of (a) bladed disk; and (b) bladed disk integrated with piezoelectric network.

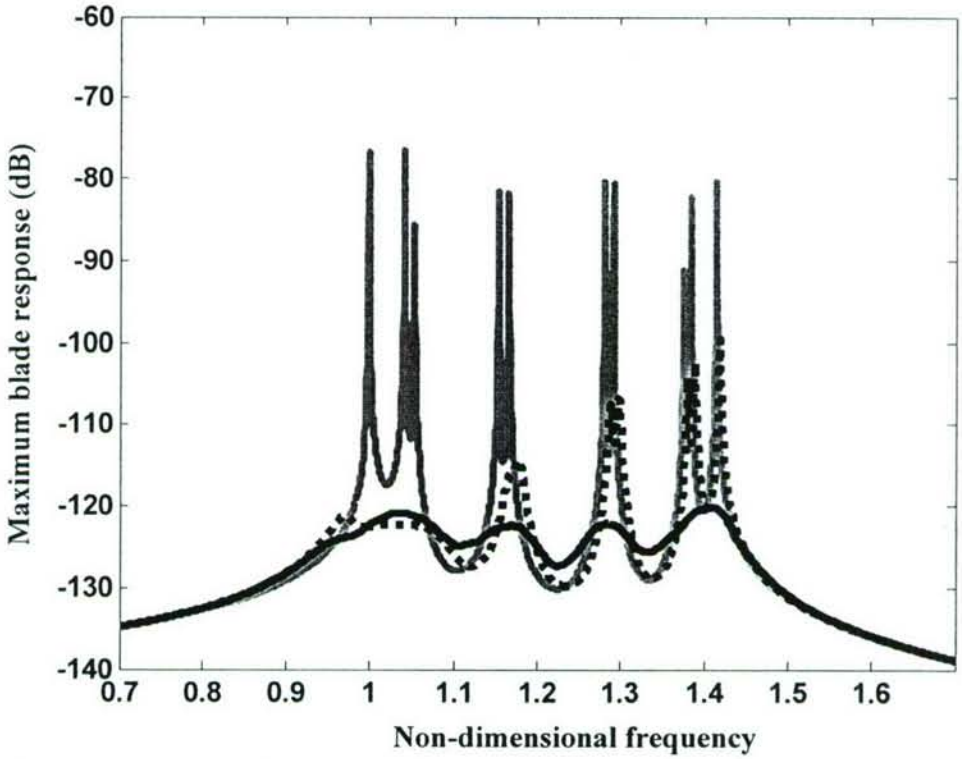

Figure 6. Comparison of suppression effectiveness between traditional absorber and optimal network. Gray solid line: without control; Black solid line: with optimal network; Black dotted line: with traditional absorber.

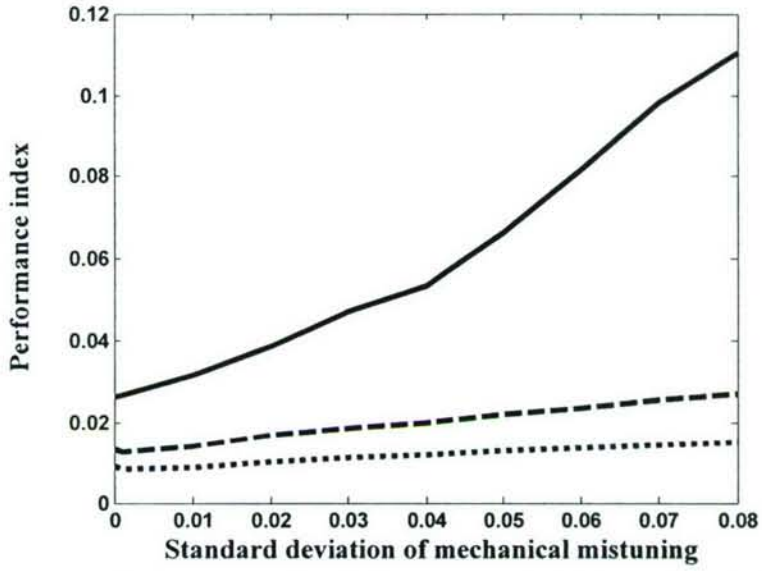

Figure 7. Performance index versus standard deviation comparison between without negative capacitance case (solid line for ξ =0.1) and with negative capacitance case (dashed line for ξ =0.2 and dotted line for ξ =0.3).

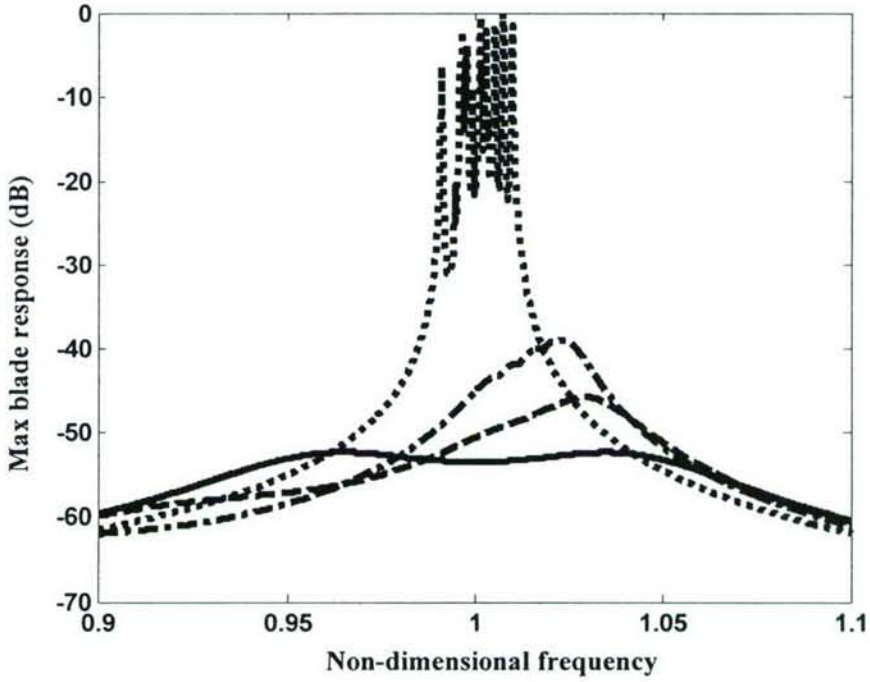

Figure 8. Maximum blade response versus frequency. Dotted line: original mechanical system without network; solid line: system with optimal tuning (δ =1.0); dashed line: system with -5% detuning (δ =0.95); dash-dotted line: system with -10% detuning (δ =0.9).

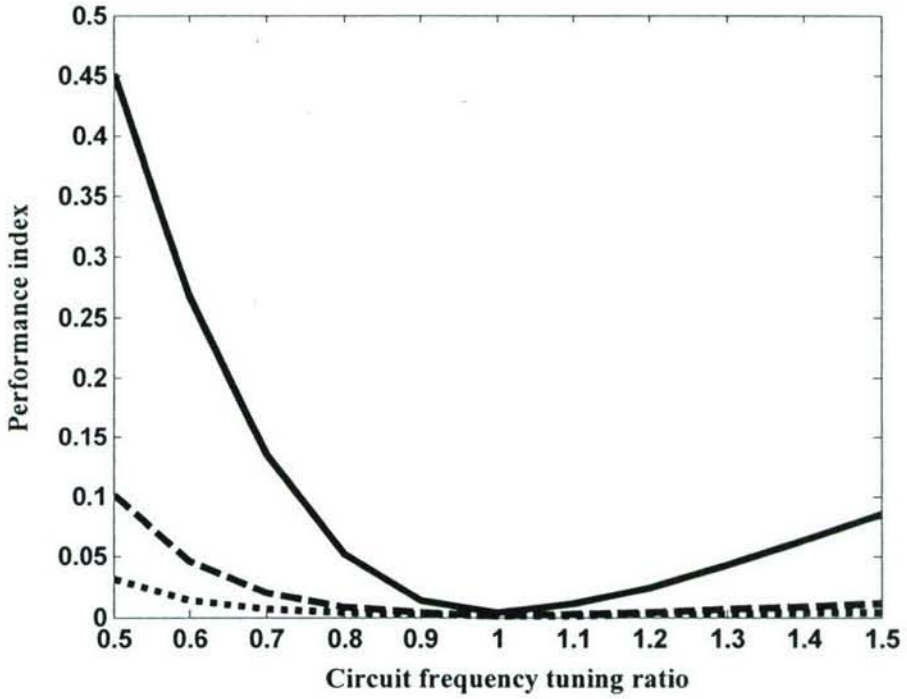

Figure 9. Detuning effect of circuit frequency tuning ratio δ on the performance, without negative capacitance (solid line for $\xi = 0.1$) and with negative capacitance (dashed line for $\xi = 0.2$ and dotted line for $\xi = 0.3$).

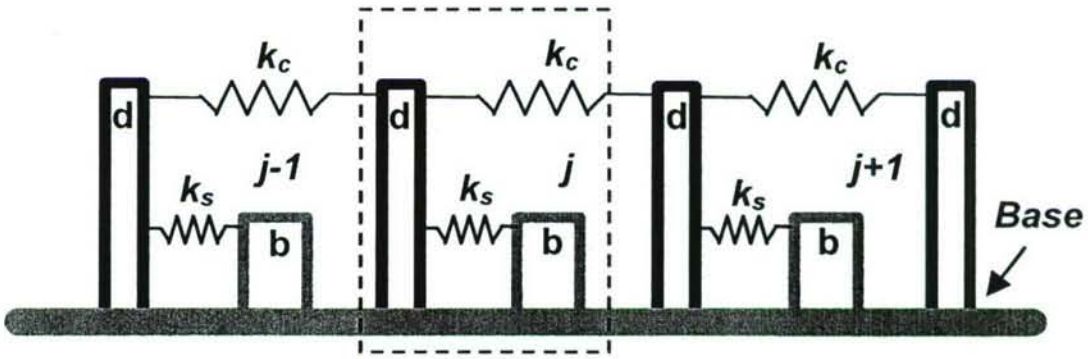

Figure 10. Complex bladed disk model with consideration of disk dynamics.

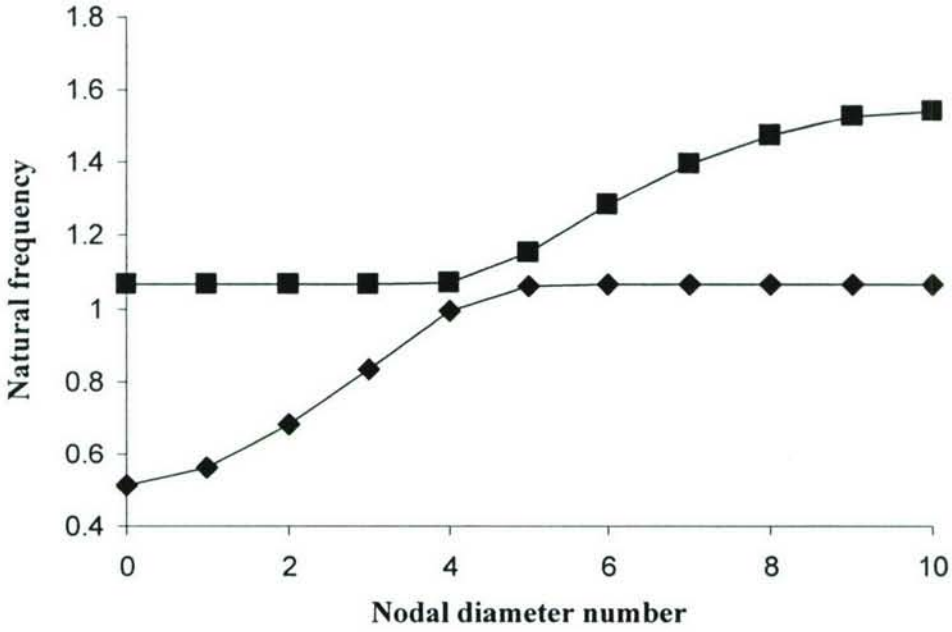

Figure 11. Curve veering characteristics of bladed-disk system.

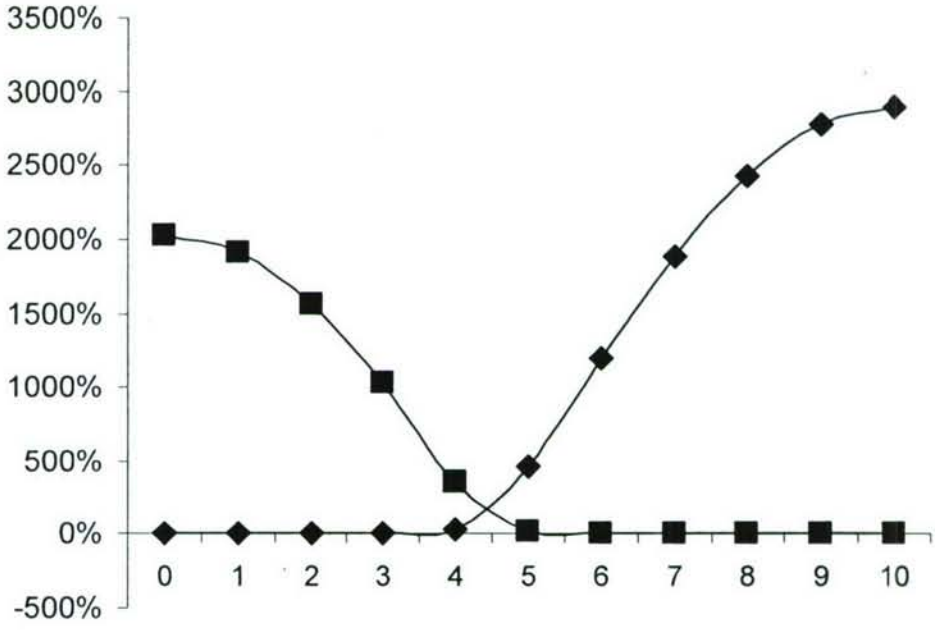

Figure 12. Blade and disk modal amplitude ratio (blade/disk).

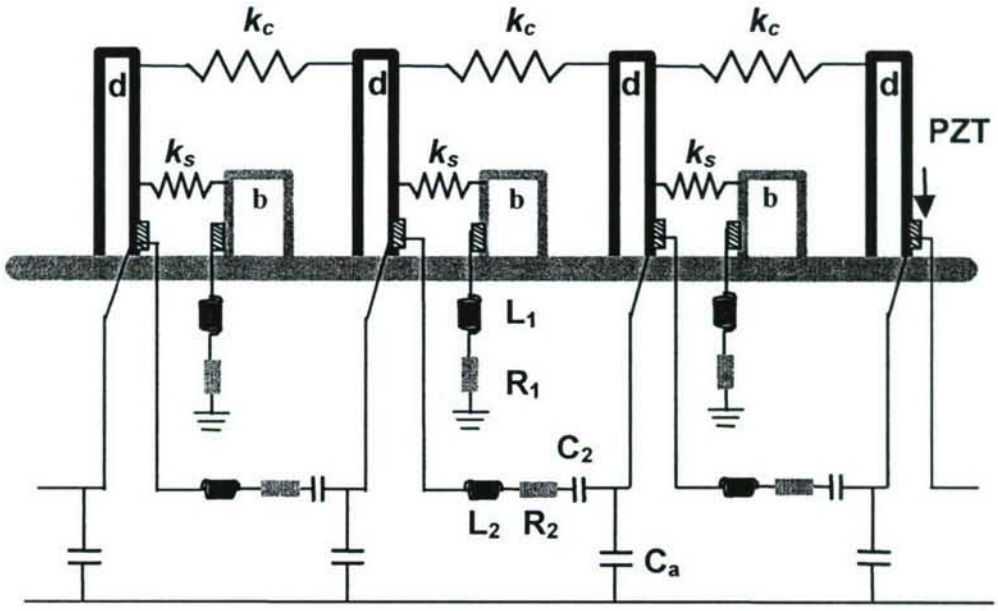

Figure 13. Bladed disk model with piezoelectric network.

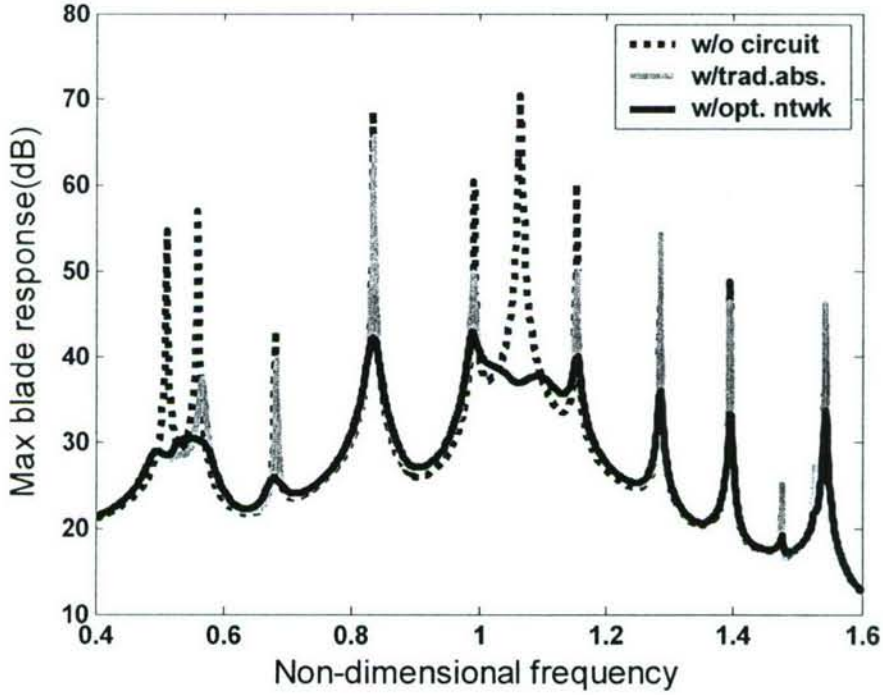

Figure 14. Maximum response of the blade-model beams versus frequency for: without circuit case, with traditional absorber case, and with the new optimal network case.

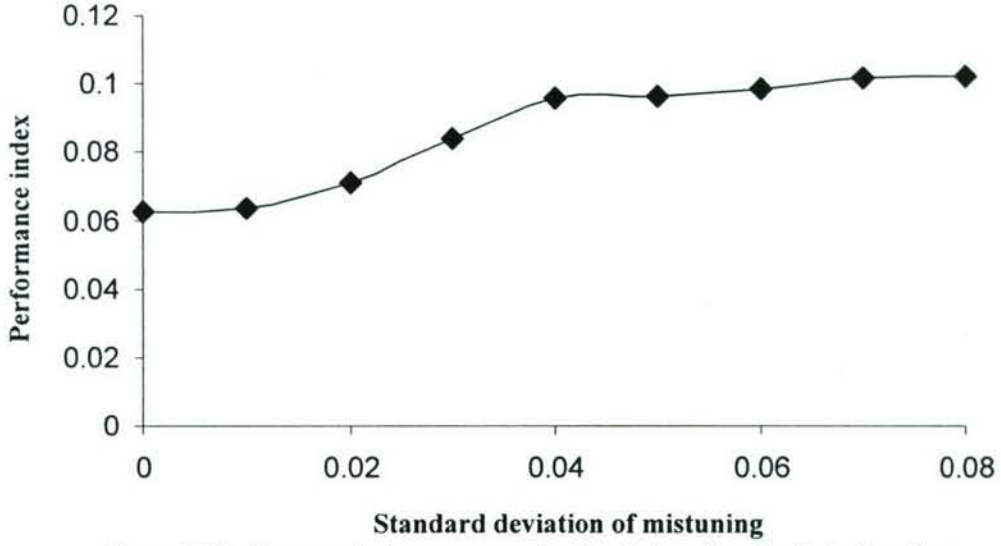

Figure 15. Performance index versus standard deviation of mechanical mistuning.

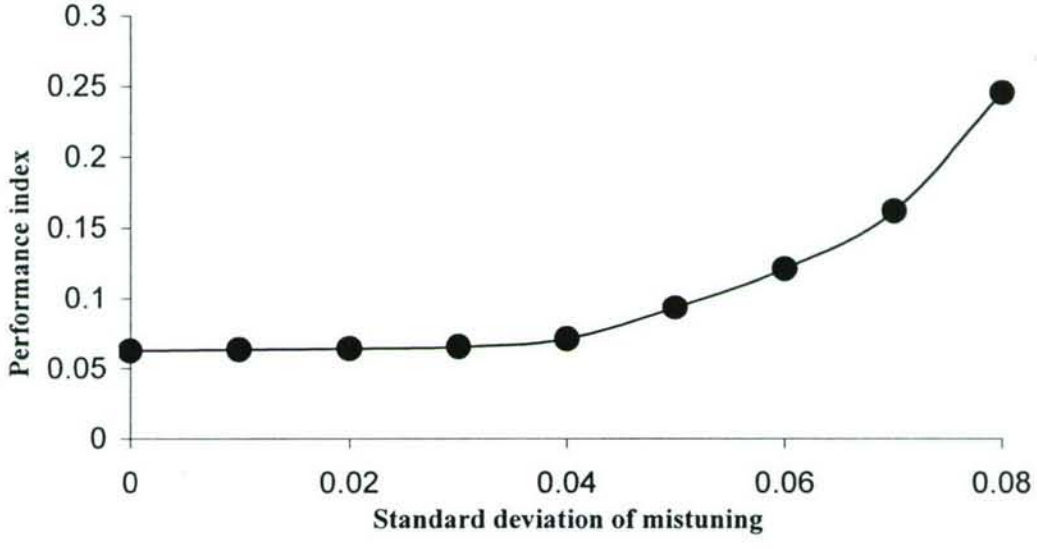

Figure 16. Performance index versus standard deviation of mistuning in circuit frequency tuning ratio δ_{el}.

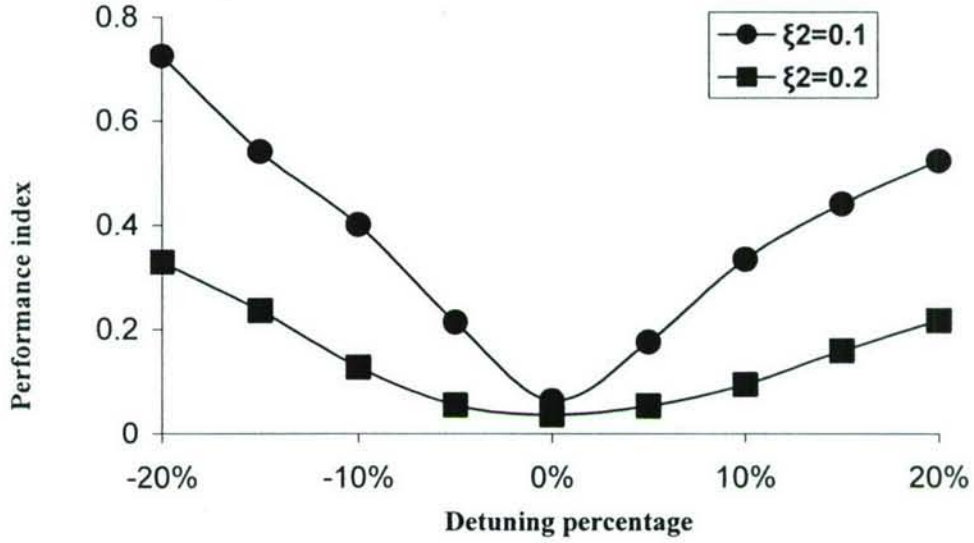

Figure 17. Performance comparison with detuning in δ_{e2} for the cases of without negative capacitance (ξ_2=0.1, ●) and with negative capacitance (ξ_2=0.2, ■).

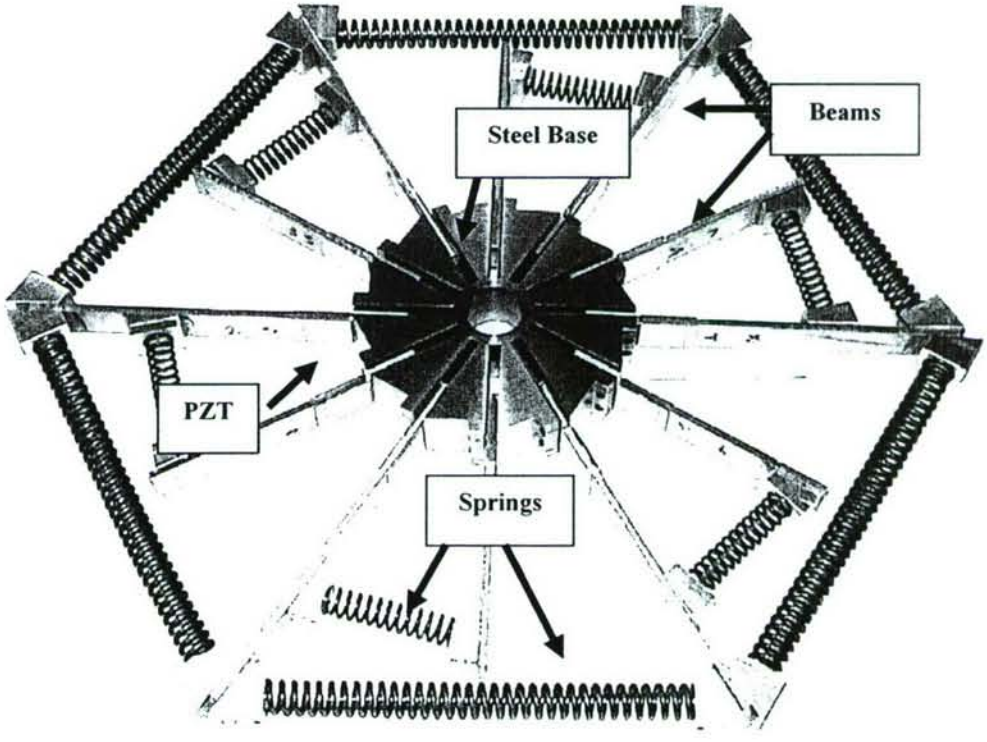

Figure 18. Baseline bladed disk model system with piezoelectric patches.

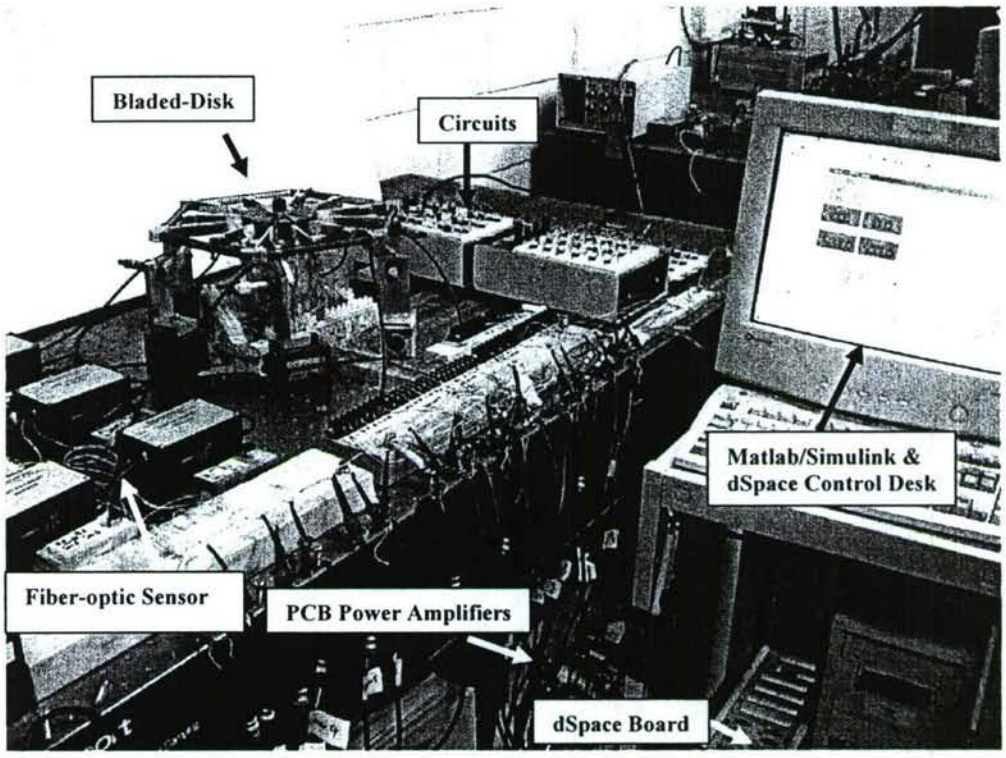

Figure 19. Overall experiment setup for vibration suppression study.

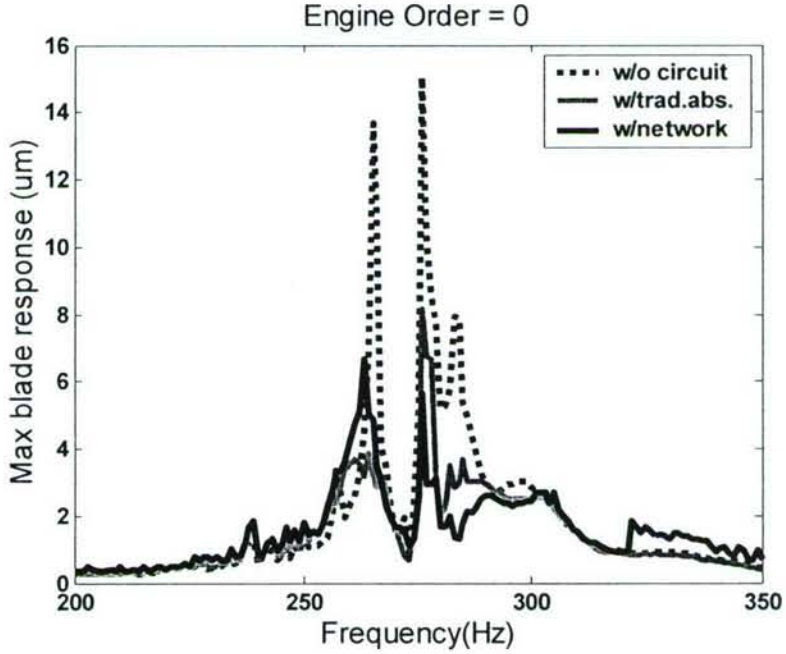

Figure 20. Maximum blade response vs. frequency for without circuit case (dotted line), with traditional absorber case (grey solid line) and with network case (black solid line) under engine order 0 excitation.

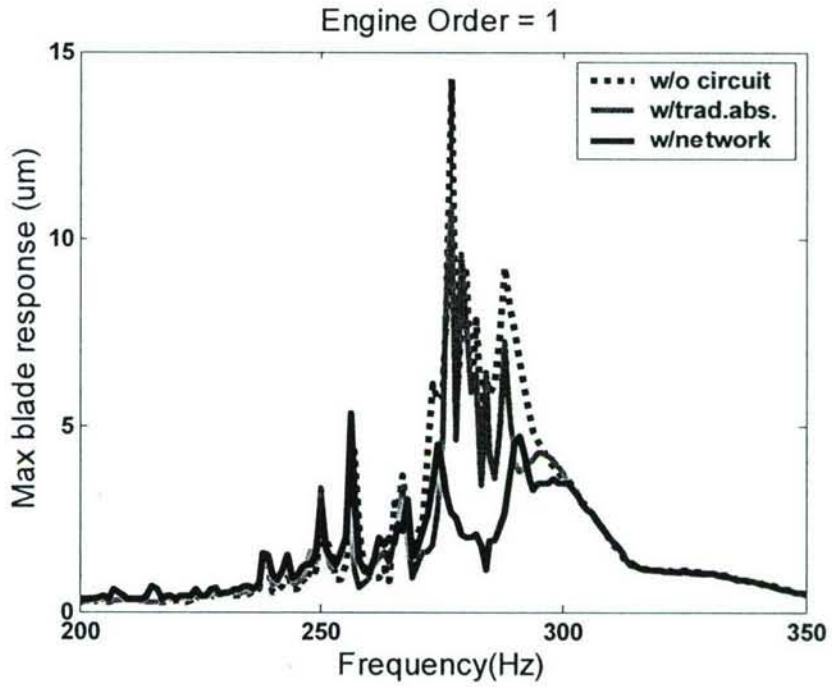

Figure 21. Maximum blade response vs. frequency for without circuit case (dotted line), with traditional absorber case (grey solid line) and with network case (black solid line) under engine order 1 excitation.

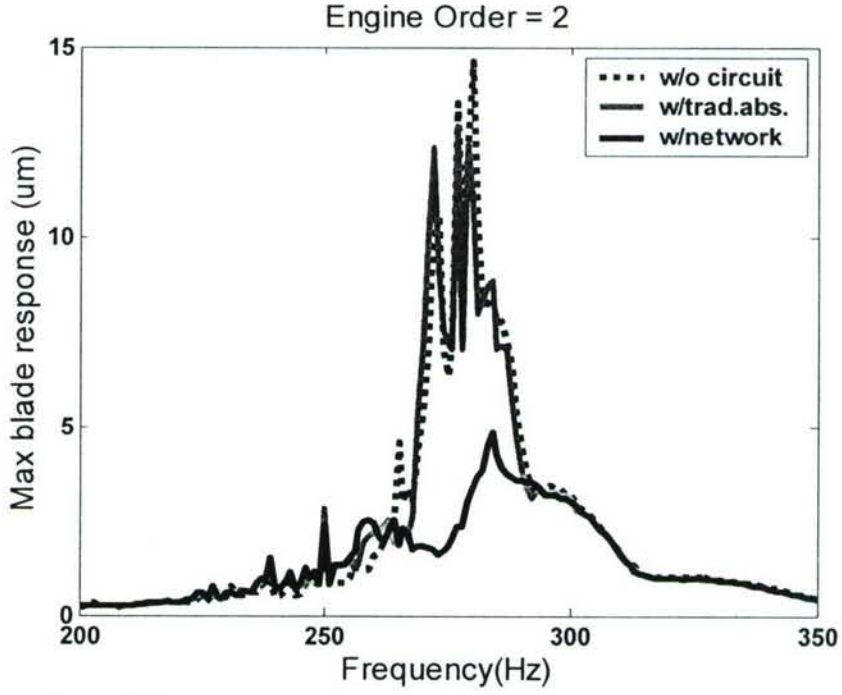

Figure 22. Maximum blade response vs. frequency for without circuit case (dotted line), with traditional absorber case (grey solid line) and with network case (black solid line) under engine order 2 excitation.

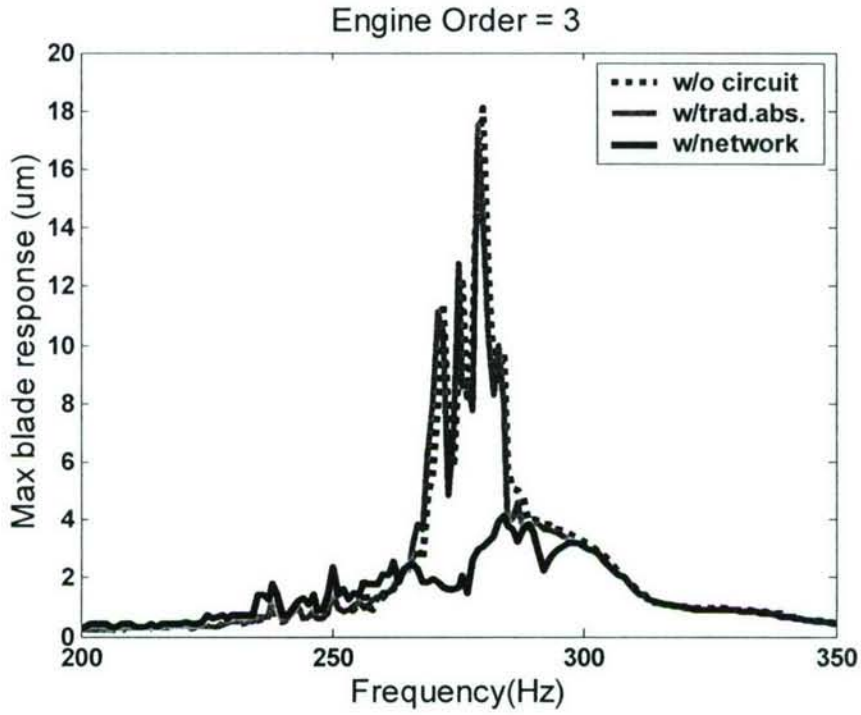

Figure 23. Maximum blade response vs. frequency for without circuit case (dotted line), with traditional absorber case (grey solid line) and with network case (black solid line) under engine order 3 excitation.